Rev. Roum. Sci. Techn.– Électrotechn. et Énerg.
Vol. **68**, *2*, pp. 188–193, Bucarest, 2023

NOVEL ROTOR POSITION EXTRACTION BASED ON ROTATING HIGH-FREQUENCY VOLTAGE INJECTION FOR PERMANENT MAGNET SYNCHRONOUS MACHINE DRIVES AT LOW OR ZERO SPEEDS

OUIZA TOUDERT[1], FRANÇOIS AUGER[2], AZZEDINE HOUARI[2], MOURAD LAGHROUCHE[1]

Keywords: Sensorless control; High frequency (HF) rotating carrier-signal injection; Surface-mounted permanent-magnet synchronous machines (SPMSM); Demodulation.

A new procedure for rotor position extraction of salient-pole permanent magnet synchronous motors (PMSM) is presented in this paper. A carrier rotating signal is injected into the machine to measure its displacement using a high-frequency current. This method reduces computation time, simplifies the extraction model, and improves the displacement assessment error. This method is effective for surface mounted-permanent magnet synchronous motors (SPMSM) exhibiting small magnetic saliencies with sinusoidally distributed stator winding supplied by a space vector pulse wide modulation (SVPWM) voltage source inverter. The experimental results proved that the online phase shift compensation method could assess the rotor displacement, the speed, and the sensorless PMSM vector control operation with high accuracy. This method has shown its effectiveness for static and dynamic performance under various operating load conditions.

1. INTRODUCTION

Due to their high torque density and efficiency, permanent-magnet synchronous motors (PMSM) are widely used in many speed control applications [1,2]. Explicit position sensors (e.g. encoders and resolvers) are usually used to obtain real-time information on the rotor position for field orientation, closed-loop speed, and position control of PMSM [1, 3]. However, the major drawback of such sensors is their large size, high cost, and complexity of the whole system. Moreover, they impair the reliability of drive systems [1]. The substitution of the position sensors by advanced algorithms embedded in the controls hardware and software has become an important topic of study in recent decades. The classical sensorless field-orientation controls used for the PMSM are categorized into two classes: The first is based on the back-EMF estimation [4,5] using some estimators such as state observers and Kalman filters [6]. Although the sensorless control in the first class is well mastered at medium to high velocities, it remains a challenging task at low velocities. The reason is that observability degenerates at zero velocity, causing a serious problem such as an error that may be induced on the rotor position assessment [7,8] and instability regarding its speed control [7]. The second class is based on magnetic saliency. It attempts to solve this problem using frequency modulation, making the system observable whatever the fundamental excitation [7,8]. Its major asset comes from its ability to estimate rotor position at low speeds and standstill. The accuracies of the position and velocity estimation in any machine are affected by the non-linearity of pulse-width modulation, the machine's dynamic behavior, the kind of carrier signal injected, and the signal processing required for the estimation.

The classical open loop carrier signal injection is impacted by the nonlinear inverter properties, such as the dead time effect, introducing errors on the mean value of the voltage, which can be compensated by several methods, such as a matrix converter using the space modulation profiling technique [9]. Another method involves adopting HF square-wave voltage injection algorithm without compensation [10].

Regarding sensorless control at vector control mode, the generated starting torque depends on the accuracy of the initial rotor position estimation. If the initial position error is comparatively large, the loading capacity at the starting stage will be limited and even causes the machine to reverse [11].

The pattern of the high-frequency signal injection is classified into: the sinusoidal circular vector [8], the sinusoidal elliptic vector [12], the sinusoidal pulsating vector [11–13], and the square wave vector [1–14,15]. They can be used in different references, such as the stationary reference frame or the estimated synchronous reference frame. The sinusoidal-wave signal injection strategy is easy and simple [1]. The pulsating injection method is more accurate and less sensitive to the power device dead-time effect than the rotating injection method [16]. However, it may face the problems of long convergence time and limited system stability. To overcome these problems, a direct signal demodulation method is proposed in [16,17]. The use of a square-wave method reduces the time delay.

Moreover, it remarkably enhances the bandwidth of position estimation and current regulation [18]. It has two main drawbacks, one of which is that the carrier injection voltage needs to increase with the increase of injection frequency to maintain a reasonable signal-to-noise(S/N) ratio. The second drawback is the need for complex signal demodulation, unlike the conventional sinusoidal signal injection methods. Therefore, some authors have proposed a novel square-wave carrier signal injection strategy using zero sequence carrier voltage [1].

Regarding the position information in the negative sequence term of the current, some signal processing must be done, including heterodyne detection. Three techniques for current demodulation can be found in the literature when the high-frequency sinusoidal circular voltage is injected into the motor [19]: the two successive synchronous reference frame filters, the analog and synchronous reference frame filters, and the single low-pass synchronous frame filters.

The drawbacks of the first one are its slow response time due to the first-order filters and the inability to eliminate the perturbations near the carrier pulsation components. Moreover, the need to use the synchronous pulsation ω_s may lead to instability [19]. The second method is the conventional solution to extract the negative sequence current component by combining three continuous time filters (a band-pass filter, a high-pass filter, and a low-pass

[1]Mouloud Mammeri University, Tizi-Ouzou, Algeria. E-mail: ouiza.toudertmansouri@ummto.dz
[2]Nantes University, IREENA Laboratory, Nantes, France. E-mail: francois.auger@univ-nantes.fr, azeddine.houari@univ-nantes.fr
[3]Lampa laboratory, Mouloud Mammeri University, Tizi Ouzou, Algeria, larouche_67@yahoo.fr

one). However, its limitations lie in its complexity, a time delay of the rotor position or speed, and a limitation of current bandwidth [19,20].

In this paper, the third structure is developed and studied. Using solely one continuous-time low-pass filter and one frequency shift is more appropriate and simpler. Furthermore, the phase shift of the adopted filter is corrected, so its estimated bias position will be nullified. This procedure has proved its efficiency in rotor position estimation on a wide operating range at low velocity. In this study, the position estimation arises from a high-frequency current injection, then the position estimation bias is eliminated through the phase correction technique.

This new method significantly simplifies signal demodulation and improves position accuracy. Moreover, it increases the position estimation robustness. The main contributions of our work include:

- A new method significantly simplifies the signal demodulation process for assessing rotor position, which leads to a lower implementation processing time.
- A new design compensation of the filter phase shift scheme considers the operating speed.
- An experimental test bench is carried out to validate the proposed method.

The rest of the paper is organized as follows. In section 2, a simplified PMSM model for high-frequency voltage injection is developed. The classically used demodulation process at the high-frequency component of the complex current signal is analyzed, then a new one is presented and described in section 3. Section 4 introduces the rotor position assessor and an advanced filter phase shift correcting technique. The comparison results between the simulation and the experimental recordings on a test bench using a dSPACE rapid prototyping system are highlighted in section 5. Finally, the conclusion is reported in section 6.

2. MATHEMATICAL MODEL OF THE PMSM UNDER HIGH-FREQUENCY VOLTAGE EXCITATION

The d-q model for a PM synchronous machine is appropriate to describe the methodology prescribed. With the expectation that only a single sinusoidal distributed saliency is considered in the machine and with sinusoidally distributed stator winding. The stator voltage model in the rotor reference frame is as follows:

$$\begin{bmatrix} V_d \\ V_q \end{bmatrix} = \begin{bmatrix} r_s & 0 \\ 0 & r_s \end{bmatrix} \begin{bmatrix} i_d \\ i_q \end{bmatrix} + \begin{bmatrix} s & -\omega_r \\ \omega_r & s \end{bmatrix} \begin{bmatrix} \phi_d \\ \phi_q \end{bmatrix}. \quad (1)$$

and the magnetic flux is as follows:

$$\begin{bmatrix} \phi_{\mathrm{d}} \\ \phi_q \end{bmatrix} = \begin{bmatrix} L_d & 0 \\ 0 & L_q \end{bmatrix} \begin{bmatrix} i_d \\ i_q \end{bmatrix} + \begin{bmatrix} \phi_{\mathrm{m}} \\ 0 \end{bmatrix}. \quad (2)$$

When converted to a stationary reference frame, the described expression may be reformulated as [9]:

$$\begin{bmatrix} v_\alpha \\ v_\beta \end{bmatrix} = r_s \begin{bmatrix} i_\alpha \\ i_\beta \end{bmatrix} + \frac{\mathrm{d}}{\mathrm{d}t} \begin{bmatrix} \phi_\alpha \\ \phi_\beta \end{bmatrix}. \quad (3)$$

with $$\begin{bmatrix} \phi_\alpha \\ \phi_\beta \end{bmatrix} = L_{\alpha\beta}(\theta_r) \begin{bmatrix} i_\alpha \\ i_\beta \end{bmatrix} + \phi_m \begin{bmatrix} \cos(\theta_r) \\ \sin(\theta_r) \end{bmatrix}. \quad (4)$$

and $$L_{\alpha\beta}(\theta_r) = \begin{bmatrix} L - \Delta L \cos(2\theta_r) & -\Delta L \sin(2\theta_r) \\ -\Delta L \sin(2\theta_r) & L + \Delta L \cos(2\theta_r) \end{bmatrix}. \quad (5)$$

where: v_α, v_β, i_α, i_β, ϕ_α and ϕ_β are respectively the voltages, the currents, and the fluxes in the stationary reference frame. $L = (L_d + L_q)/2$ and $\Delta L = (L_d - L_q)/2$ are the average inductance and the zero-to-peak differential inductance respectively.

The machine is used to produce an electromagnetic torque given by:

$$T_e = \mathrm{p}[\phi_m + (L_q - L_d) i_d] i_q. \quad (6)$$

The generated torque permits to control the provided speed as the following equation expresses it:

$$\mathrm{J} \frac{\mathrm{d}}{\mathrm{d}t} \omega_r + f \omega_{\mathrm{r}} = T_e - T_r. \quad (7)$$

In this regard, the generated electromagnetic torque can be exploited to correct the load torque with the friction losses and vary the generated speed.

By supplying the voltages source inverter with the space vector modulation (SVM), the balanced sinusoidal signals with high frequency and low amplitude can be superimposed to the fundamental excitation of the PMSM motor terminals [20, 21]:

$$V_{\alpha\beta\_c} = \begin{bmatrix} v_{\alpha\_c} \\ v_{\beta\_c} \end{bmatrix} = \begin{bmatrix} -V_c \sin(\omega_c t) \\ V_c \cos(\omega_c t) \end{bmatrix} = V_c \mathrm{e}^{\mathrm{j}\left(\omega_c t + \frac{\pi}{2}\right)}. \quad (8)$$

where: v_{α_c} and v_{β_c} are the high-frequency voltages components, respectively. The pulsation $\omega_c = 2\pi f_c$. The need gives the minimum frequency for frequency separation due to the filtering, and the maximum frequency is given by the limitations of the switching frequency (f_c around 1 kHz) and the magnitude V_c (in the order of 10 V) of the selected carrier signal are retained [21].

At high frequency, the prescribed model PMSM eq. (3)-(4) may be reduced to

$$\begin{bmatrix} v_{\alpha\_c} \\ v_{\beta\_c} \end{bmatrix} = \left(r_s I_2 + \frac{\mathrm{d}}{\mathrm{d}t} L_{\alpha\beta}(\theta_r) \right) \begin{bmatrix} i_{\alpha\_c} \\ i_{\beta\_c} \end{bmatrix} + L_{\alpha\beta}(\theta_r) \frac{\mathrm{d}}{\mathrm{d}t} \begin{bmatrix} i_{\alpha\_c} \\ i_{\beta\_c} \end{bmatrix} \approx L_{\alpha\beta}(\theta_r) \frac{\mathrm{d}}{\mathrm{d}t} \begin{bmatrix} i_{\alpha\_c} \\ i_{\beta\_c} \end{bmatrix} \quad (9)$$

where: I_2 is the two-dimensional identity matrix. Equation (9) proves that the high-frequency current components in the stationary reference frame i_{α_c} and i_{β_c} are generated by this carrier voltage injection. Hence three components can be associated with the stator current: a positive sequence component following the rotation of the injected voltage, a negative sequence component following the inverse rotation of the injected voltage, and a low-frequency component ($i_{\alpha\beta\_s}$) produced by the low-frequency monitoring voltage, the stator flux and the rotor flux:

$$i_{\alpha\beta} \approx I_{cp} \mathrm{e}^{\mathrm{j}\left(\omega_c t - \frac{\pi}{2}\right)} + I_{cn} \mathrm{e}^{\mathrm{j}\left(-\omega_c t + 2\theta_r + \frac{\pi}{2}\right)} + i_{\alpha\beta\_s}. \quad (10)$$

The magnitude of the positive sequence part is:

$$I_{cp} = \frac{L V_c}{(L^2 - \Delta L^2)\, \omega_c}. \quad (11)$$

The magnitude of the negative sequence part is:

$$I_{cn} = \frac{\Delta L V_c}{(L^2 - \Delta L^2)(\omega_c - 2\omega_r)}. \quad (12)$$

From eq. (10), it can be noticed that the indication regarding the rotor position is included in the second term θ_r. Therefore, a corresponding signal-processing method must be applied to extract this component.

3. STATOR CURRENT SIGNAL PROCESSING

3.1 CLASSICAL METHOD DESCRIPTION

To extract the rotor angle information θ_r in eq. (10) and eliminate the other undesirable terms, the classical method is the most used [19, 20]. It uses an analog band-pass filter (BPF) centered on the carrier frequency f_c. The role of this filter is twofold: i) keeping both low amplitudes with high-frequency terms of the measured stator current and ii) eliminating the excitation of low-frequency current.

The estimated complex current is multiplied by $e^{-j\omega_c t}$, a heterodyning process, to realize a frequency shift of $-\omega_c$. Consequently, the negative sequence term is translated near the $-2\omega_c$. Regarding the positive sequence term, it is converted into a dc term, which may be eliminated through a high-pass filter. The resulting signal is multiplied by $e^{+j\omega_c t}$ to shift the negative sequence term near zero and generate a signal proportional to $e^{j2\theta_r}$. The obtained signal is passed through a low-pass filter followed by a phase extraction to extract the measured rotor position (Fig. 1).

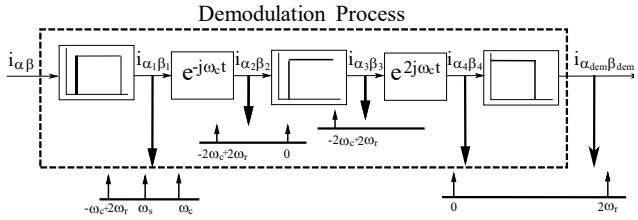

Fig. 1 – Usual procedure in assessing rotor position.

3.2 SUGGESTED PROCESSING PROCEDURE

As shown in Fig. 2, our new method first consists in multiplying the assessed stator current $i_{\alpha\beta}$ by $e^{j\omega_c t}$ to realize a frequency shift of $+\omega_c$. As a consequence, the negative sequence term is translated toward zero. The other terms are situated at a frequency band greater than the carrier one.

$$i_{\alpha\beta}e^{j\omega_c t} \approx I_{cn}e^{j\left(2\theta_r+\frac{\pi}{2}\right)}+I_{cp}e^{j\left(2\omega_c t-\frac{\pi}{2}\right)}+I_{\alpha\beta\_s}e^{j(\omega_c t)}. \quad (13)$$

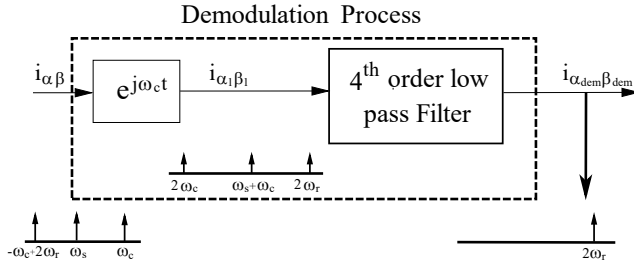

Fig. 2 – Simple demodulator suggested for assessing rotor position.

The last two components can be eliminated using a low-pass filter, rendering a new signal $i_{\alpha\, dem\, \beta dem}$ proportional to $e^{j(2\theta_r)}$, (Fig. 2) and the rotor position assessment is finally obtained by phase extraction (Fig. 4).

Bessel filters are needed for the two cases due to their maximal linear phase output, generating a displacement assessment error proportional to the rotor speed. The different coefficients are calculated as it is done in [22]. The proposed procedure uses A fourth-order low-pass filter to reduce the low-frequency excitation fraction. This filter is designed by combining two second-order Bessel low-pass filters in series.

Figure 3 illustrates the frequency response of both demodulators. It can be seen that they are exhibiting similar bandwidth ($\pm$40Hz in the vicinity of -1000 Hz). The usual demodulation process presents an ideal rejection around DC and +1000 Hz, but the adopted procedure presents more attenuation everywhere else. Figure 3 illustrates that the phase declivity near -1000 Hz is greater in the suggested demodulator than in the usual procedure. Therefore, a phase-correcting technique is needed.

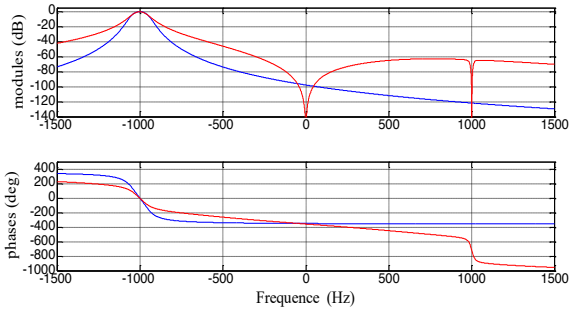

Fig. 3 – Frequency responses of the suggested (blue line) and the usual demodulators (red line).

4. UNBIASED SPEED AND POSITION ASSESSMENT

4.1 SPEED AND POSITION ASSESSOR

The demodulation realized on the negative sequence component provides the signals $I_{cn}\cos(2\theta_r)$ and $I_{cn}\sin(2\theta_r)$. An inverse tangent function can evaluate The rotor position from the above signals. Still, more denoised estimation is realized with a non-linear second-order angle tracking observer [8], appropriate in this case as illustrated in Fig. 4. This observer presents an evaluation of the location ($\hat{\theta}_r$) and speed ($\hat{\omega}_r$) of the rotor. From the maximal electromagnetic torque of the machine $T_{e\,max}$, the maximal angular acceleration is expressed as:

$$\alpha = \frac{T_{e\,max}}{J}. \quad (14)$$

The first-factor K_b (see Fig. 4) can be chosen as

$$K_b = \frac{\alpha}{\tilde{\theta}_{r\_max}}. \quad (15)$$

The term $\tilde{\theta}_{r\_max}$ represents the acceptable upper limit on the position assessment error arising from that angular acceleration. The other factor K_a is formulated as

$$K_a = 2m\sqrt{K_b}. \quad (16)$$

where: m is a damping ratio chosen by the user. This parameter can be chosen to obtain a desired peak overshoot when the actual rotor position abruptly changes. For example, choosing an overshoot of 5% leads to $m = 1.945$ [23].

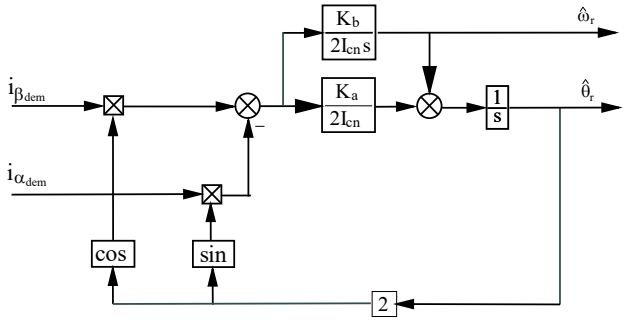

Fig. 4 – Overview drawing of the nonlinear second-order angle tracking observer.

4.2 CORRECTION OF THE POSITION ESTIMATION ERROR

This procedure proved that the biased rotor assessment is attained (Fig. 4) when the angle tracking observer verifies the negative sequence terms extractor (Fig. 1 or Fig. 2). This bias is due to the phase shift $\varphi(\omega)$ of the filters adopted in the demodulation step. The expressions of these phase shifts are known, and the angle-tracking observer also estimates the rotor speed. This correcting technique is detailed by the overview drawing of Fig. 5, where $\varphi_{LP4}(\omega)$ is the argument of the fourth-order low-pass filter adopted in the demodulation process and is given by the eq. 17.

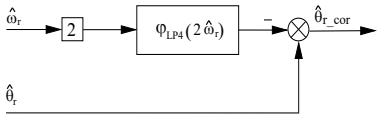

Fig. 5 – Adopted estimation error correction procedure.

$$\varphi_{LP4}(\omega) = \operatorname{atan2}(-2m_1\omega_{b1}\hat{\omega}\,,\omega_{b1}^2-\hat{\omega}^2) + \operatorname{atan2}(-2m_2\omega_{b2}\hat{\omega}\,,\omega_{b2}^2-\hat{\omega}^2) \quad (17)$$

where: m_1, m_2, ω_{b1}, and ω_{b2} are the Bessel low pass-filter coefficients given in [22].

5. SIMULATION AND EXPERIMENTAL RESULTS

To evaluate the effectiveness of the proposed method for sensorless low and zero-speed operation of PMSM, a set of simulations was performed on MATLAB/Simulink and a test bench was used for experimental tests. The parameters of the simulated machine are based on the identification of an industrial 4.4 kW SPMSM (Yaskawa SGMGH-44DCA6F) shown in Table I. The motor is supplied by a power converter controlled by the space vector modulation technique (SVM). The output voltage reference is calculated like in [24], receiving three monitor signals delivered by a classical vector monitor arising from three PI controllers and tuned by the symmetrical optimum method [25]. The speed and position estimation uses an extractor and demodulator operating in the negative sequence part, an angle tracking observer, and a phase shift corrector, as depicted in Fig. 6.

The experiments are implemented on a dSPACE dS1103 control system (100 µs sampling period), which is composed of the computer, the dSPACE boards, the inverter, the PMSM, the load machine used to generate a mechanical load torque, the current sensor, the voltage sensor, and the incremental position encoder sensor. Figure 7 shows the photograph of the test bench used in the experimental tests. Figure 8 shows the comparison between the simulated and the experimental rotor position estimation error, obtained with the proposed method under no load, when the two references of the speed controller are a step-change, changing from standstill to 10 rad/s and 20 rad/s. It can be seen that the simulation results tally closely with the experimental ones without correction. The estimation error is augmented with the rotor speed. This can generate instability in the speed regulation since the estimated position is appeared in the abc/dq and dq/αβ relation in the vector control, as illustrated in Fig. 6.

The corresponding phase shift introduced by the filter used in the demodulation process is illustrated in Fig. 9. As one can notice, it increases proportionally with the reference speed because, at low speeds, eq. 17 can be approximated by a straight. Figure 10 presents the real speed attained when the speed-reference command varies drastically from standstill to 10 rad/s and -10 rad/s. This figure proves that the PI regulator of the speed has been fixed at the current speed to fit the set speed. Figure 11 illustrates the speed assessment error, and Fig. 12 shows a zoom of the rotor position assessment.

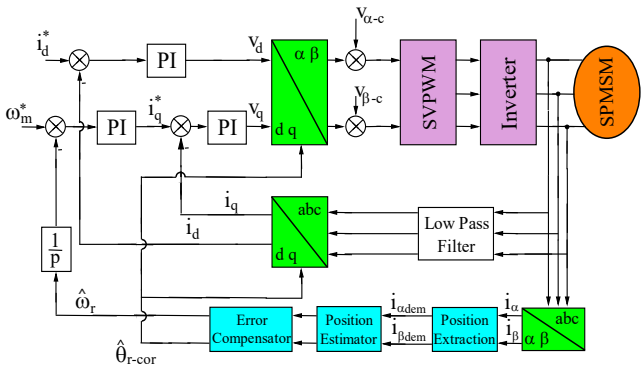

Fig. 6 – Block diagram of the sensorless vector control of a salient PMSM using high-frequency signal injection.

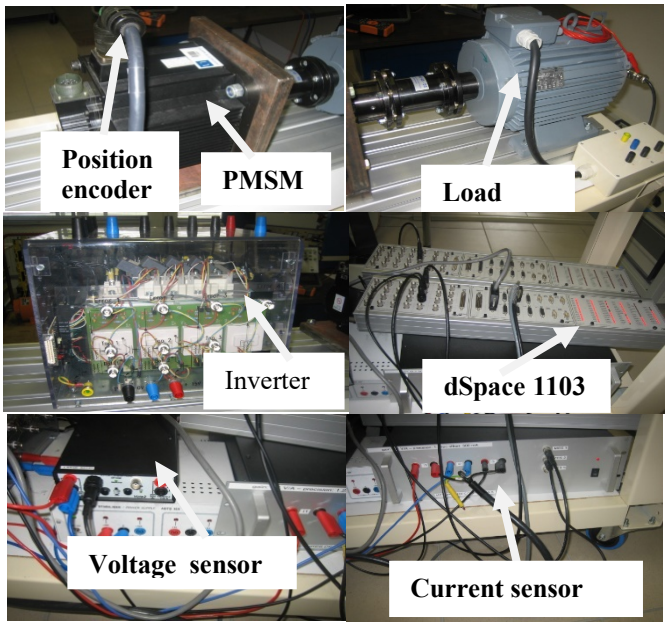

Fig.7 – Experimental test bench.

As shown in Fig. 13, before the phase shift compensation, the electrical position error estimation averaged 15°. Whereas, after compensation, the estimation error remains below ±5° when the speed reference is 10 rad/s and ±5° when the speed reference is −10 rad/s. It implies that with the suggested procedure, a very stable speed regulation is achieved at the expense of a simpler demodulator.

The dynamic position estimation performance with the proposed method is also tested with a load of about 1 Nm; the speed-reference command is steadily fixed at 15 rad/s. The estimated speed and position are depicted respectively in Fig. 14 and Fig. 15. The controlled speed and position follow the current ones of the machine along with the estimated speed and position. Figure 15 shows that the electrical estimation position error is reduced from 32 ° without phase compensation to 3° by using the compensation scheme.

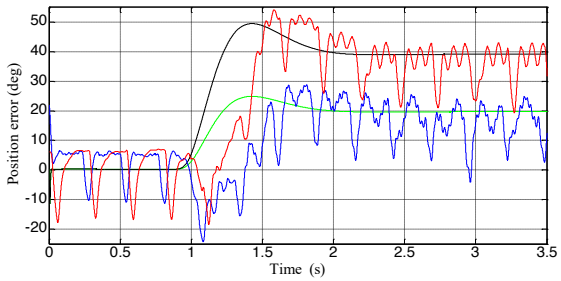

Fig. 8 – Position estimation error using the suggested procedure without phase shift correction with the step speed references (blue and red lines: experimental curve with step speed equal to 10 rad/s and 20 rad/s, green and black lines: a simulated curve with step speed equal to 10 rad/s and 20 rad/s).

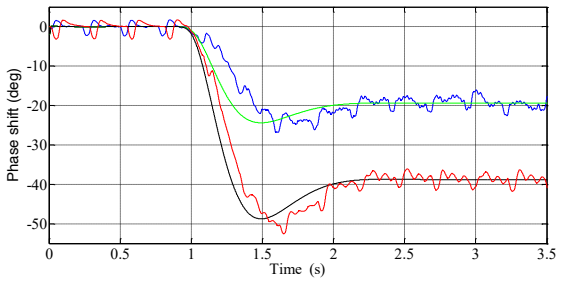

Fig. 9 –Phase shifts (blue and red lines: experimental curve with step speed equal to 10 rad/s and 20 rad/s, green and black lines: simulated curve with step speed equal to 10 rad/s and 20 rad/s).

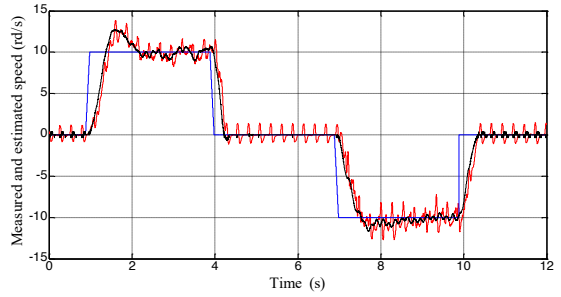

Fig. 10 –Rotor speed (blue line: desired, red line: estimated, black line: measured).

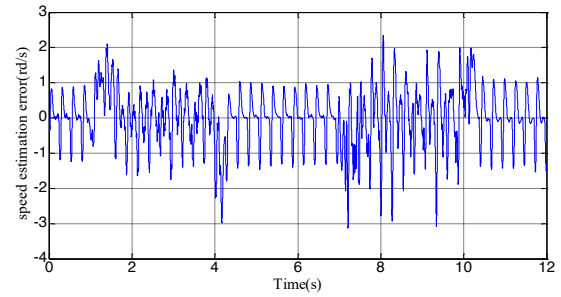

Fig. 11 – Speed estimation error.

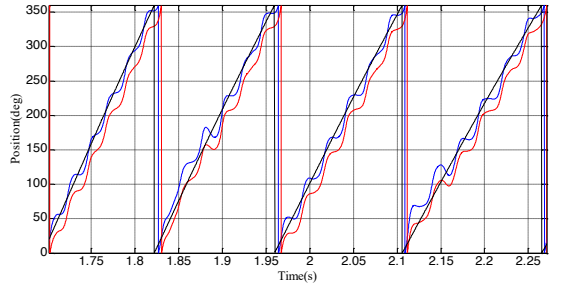

Fig. 12 –A zoom of electrical position estimation (blue line: with compensation, red line: without compensation, black line: measured).

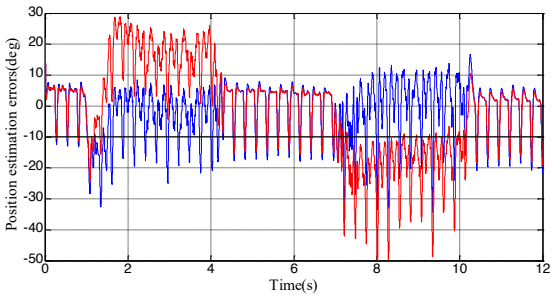

Fig. 13 – Position estimation error using the suggested procedure without and with considering the phase correction (blue line: with compensation, red line: without compensation).

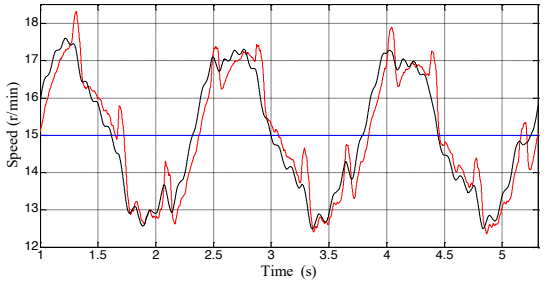

Fig. 14 – Rotor speed under a load torque (blue line: desired, red line: estimated, black line: measured).

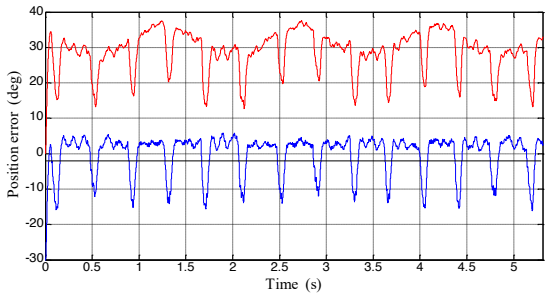

Fig. 15 – Position estimation error using the suggested procedure when a load torque fixed at 1 Nm is applied (blue line: with compensation, red line: without compensation).

6. CONCLUSION

A new rotor position assessor of the surface-mounted permanent magnet synchronous machine (SPMSM) using rotational sinusoidal signal injection is presented. To identify the negative sequence of the current containing the position indication, the commonly used procedure usually includes of three analog filters. The adopted procedure is more appealing regarding signal processing since it utilizes solely one analog filter. It is cost-effective and imparts short processing time. It has been proved that the filter phase shift is closely linked to the working speed. The filter phase shift decreases considerably when the working speed is considered in the correction technique, hence imparting a precise rotor displacement assessment. Experimental results presented in the paper corroborated with the simulation approach and proved the effectiveness of the suggested procedure for low speed, including reversal speed, in the load condition. Despite the reversal saliency of the machine and its reduced dimensions $\left(L_q/L_d = 0.5\right)$ compared to the IPMSM, it is still sufficient to assess the rotor speed and position. The injected signal frequency causes electromagnetic and acoustic noises. The results achieved here are with low load; further work will include implementations at various heavy loads.

Table 1
Motor model parameters

Parameter	Value
Rated flux	0.32 Wb
Rated output power	4.4 kW
Rated torque	28.4 Nm
Inertia	0.0151 kg.m^2
Rated speed	1500 r/min
Rated voltage	400 V
Rated current	16.5 A
r_s	0.25 Ω
L_d	4.8 mH
L_q	4.1 mH
p	4

SYMBOLS and ABBREVIATIONS

L_d, L_q : d-axis and q-axis stator inductance (H).
r_s : stator resistance (Ω).
v_α, v_β, i_α, i_β: voltages and currents in the stationary reference frame.
v_a, v_b, v_c, i_a, i_b, i_c: voltages and currents in the abc reference frame.
v_d, v_q, i_d, i_q: voltages and currents in the dq reference frame.
s: differential operator d/dt (Laplace variable).
θ_r and $\hat{\theta}_r$: actual and estimated electrical angles between the stator q-axis and the rotor q-axis (rad).
ω_r and $\hat{\omega}_r$: actual and estimated velocity of the fundamental electrical excitation (rad/s).
V_c, ω_c and f_c: magnitude (V), angular frequency (rad/s), and frequency (Hz) of injected high-frequency voltage, respectively.
ω_m : mechanical rotor speed (rad/s).
ω_m^* : desired mechanical rotor speed (rad/s).
ϕ_m : constant flux linkage due to the permanent magnets (V.s)
ϕ_{dq} : fluxes in the d-q reference frame
p : number of pole pairs.
J : overall inertia (kg m^2).
f : viscous friction coefficient (Nm s)
T_r : load torque (Nm).
T_e : electromagnetic torque (Nm).

Received on 16 November 2022

REFERENCES

1. P.L. Xu, Z.Q. Zhu, *Novel square-wave signal injection method using zero sequence voltage for sensorless control of PMSM drives*, IEEE Transactions on Industrial Electronics, **63,** *12*, pp. 7444–7454 (2016).
2. J. Liu, H. Li, Y. Deng, *Torque ripple minimization of PMSM based on robust ILC via adaptative sliding mode control,* IEEE Transactions on Power Electronics, **33**, *4*, pp. 3655–3671 (2018).
3. M.I. Abdelwanis, R. El-Sehiemy, M.A. Hamida, *Parameter estimation of permanent magnet synchronous machines using particle swarm optimization algorithm*, Rev. Roum. Sci. Techn. – Électrotechn. Et Énerg., **67**, *4*, pp. 377–382 (2022).
4. A. Sarikhani, O.A. Mohammed, *Sensorless control of PM synchronous machines by physics-based EMF observer,* IEEE Transactions on Energy Conversion, **27**, *4*, pp. 1009–1017 (2012).
5. I. Boldea, M.C. Paicu, G.D. Andreescu, F. Blaabjerg, *Active flux DTFC-SVM sensorless control of IPMSM*, IEEE Transactions on Energy Conversion, **24**, *2*, pp. 314–322 (2009).
6. J.H. Jang, S. K, J. I. Ha, M. Sawamura, *Sensorless drive of surface-mounted permanent-magnet motor by high-frequency signal injection based on magnet saliency*, IEEE Transactions on Industry Applications, **39**, *4*, pp. 1031–557 (2003).
7. M. Mamo, K. Ide, M. Sawamura, J.O. Oyama, *Encoderless position estimation for symmetric cage induction machines under loaded Conditions*, IEEE Transactions on Industry Applications, **37**, *6*, pp. 1793–1800 (2001).
8. G.D. Andreescu, C.I. Pitic, F. Blaabjerg, I. Boldea, *Combined flux observer with signal injection enhancement for wide speed range sensorless direct torque control of IPMSM drives,* IEEE Transactions on Energy Conversion, **23,** *2*, pp. 393–402 (2008).
9. D. Saltiveri, A. Arias, G.Asher, M. Sumner, *Sensorless control of surface-mounted permanent magnet synchronous motors using matrix converters*, Electrical power quality and utilization journal, **12**, *1*, pp. 59–67 (2006).
10. R. Ni, D. Xu, F. Blaabjerg, K. Lu, G. Wang, G.Zhang, *Square-wave voltage injection algorithm for PMSM position sensorless control with high robustness to voltage errors,* IEEE Transactions on Power Electronics, **32**, *7*, pp. 5425–5437 (2016).
11. J. Li, B. Zhou, B. Liu, L. Wang, T. Ni, *A novel strategy of initial position detection for surface mounted permanent magnet synchronous machines*, *17th International Conference on Electrical Machines and Systems (ICEMS),* Hangzhou, China, 2014.
12. A. Jebai, F. Malrait, P. Martin, P. Rouchon, *Sensorless position estimation and control of permanent-magnet synchronous motors saturation model*, International Journal of Control, **89**, *3*, pp. 535–549 (2016).
13. X. Luo, Q. Tang, A. Shen, Q. Zhang, *PMSM sensorless control by injecting HF pulsating carrier signal into estimated fixed-frequency rotating reference frame*, IEEE Transactions on Industrial Electronics, **63**, *4*, pp. 2294–2303 (2016).
14. Y.D. Yoon, S.K. Sul, *Sensorless control of induction machines based on square-wave voltage injection*, IEEE Transactions on Power Electronics, **29**, 7, pp. 3637–3645 (2014).
15. X. Wu, Y. Feng, X. Liu, S. Huang, X. Yuan, J. Gao, J. Zheng, *Initial rotor position detection for sensorless interior PMSM with square-wave voltage injection*, IEEE Transactions on Magnetics, **53**, *11*, pp. 1–4 (2017).
16. Y.S. Jeong, R.D. Lorenz, T.M. Jahns, S.K. Sul, *Initial rotor position estimation of an interior permanent-magnet synchronous machine using carrier-frequency injection methods*, IEEE Transactions on Industry Applications, **41**, *1*, pp. 38–45 (2005).
17. X. Zhang, H. Li, S. Yang, M. Ma, *Improved initial rotor position estimation for PMSM drives based on HF pulsating voltage signal injection,* IEEE Transactions on Industrial Electronics, **65**, *6*, pp. 4702–4713 (2018).
18. S. Bolognani, S. Calligaro, R. Petrella, M. Tursini, *Sensorless control of IPM motors in the low-speed range and at a standstill by HF injection and DFT processing*, IEEE Transactions on Industry Applications, **47**, *1*, pp. 96–104 (2011).
19. L. Baghli, I. Al-Rouh, A. Rezzoug, *Signal analysis and identification for induction motor sensorless control, Control Engineering Practice*, **14**, *11*, pp. 1313–1324 (2006).
20. H. Kim, M.C. Harke, R.D. Lorenz, *Sensorless control of interior-permanent magnet machine drives with zero-phase lag position estimation*, IEEE Transactions on Industry Applications, **39**, *6*, pp. 1726–1733 (2003).
21. S. Medjmadj, D. Diallo, A. Arias, *Mechanical sensor fault-tolerant controller in PMSM drive: experimental evaluation of observers and signal injection for position estimation,* Rev. Roum. Sci. Techn. – Électrotechn. Et Énerg., **66**, *2*, pp. 77–83 (2021).
22. J. Karki, *Active low-pass filter design, Texas Instruments*, *Application report*, SLOA049B (2002).
23. F. Auger, O. Mansouri-Toudert, A. Chibah, *Design of advanced resolver-to-digital converters, 10th Electrimacs conference,* Cergy-Pontoise, France, 2011.
24. A.M. Sani, S. Filizadeh, *Digital implementation and transient simulation of space-vector modulated converters*, *Power Engineering Society General Meeting*, Montreal, Quebec, Canada, 2006.
25. L. Loron, *Tuning of PID controllers by non-symmetrical optimum method*, Automatica, **33**, *1*, pp. 103-107 (1997).